Bioresorbable phosphate glass based microstructured optical fibers with hole and core

Seyed H. Mussavi Rizi[a], Nadia Boetti[b], Diego Pugliese[a], Davide Janner[a,*]

[a] Department of Applied Science and Technology (DISAT) and RU INSTM, Politecnico di Torino, Corso Duca degli Abruzzi 24, 10129 Torino, Italy

[b] Fondazione LINKS-Leading Innovation and Knowledge for Society, via P. C. Boggio 61, 10138, Turin, Italy

Corresponding author: davide.janner@polito.it

Abstract

Bioresorbable phosphate glasses are an excellent alternative to conventional silicate-based glass systems for biomedical applications. These glasses can have tailorable bioresorbability and mechanical properties, a wide range of transparency windows (from 300 to 2600 nm), and are of great interest for biophotonic devices. The present work investigates the feasibility of fabricating a microstructured bioresorbable optical fiber combined with a microfluidic channel. Extrusion and stack-and-draw techniques are used to manufacture the microstructured optical fiber capable of guiding light and liquid simultaneously. An optimized extrusion procedure allowed fabricating performs with low bending and tapering possible. The preform was drawn to 130 and 230 μm diameter fibers. Light guide and attenuation loss were characterized, and the microfluidic channel was tested for liquid delivery. The proposed approach demonstrates the vast potentiality of such microstructured fiber that could be used as a theranostics device to be employed in specific areas inside the body without needing a removal procedure.

Keywords: calcium-phosphate glass; microstructured optical fiber; glass extrusion; bioresorbable fiber optics

1. Introduction

The use of glass systems in the biomedical field dates back to 1971 when Hench et al. invented BioGlass, which later became known as 45S5 bioactive glass [1]. Biomedical researchers have extensively examined different glass compositions, phosphate glass (PG) systems being among the best known. In bulk or fiber form, calcium-phosphate systems have been successfully used as scaffolds in soft and hard tissue engineering for a long time [2,3,12–16,4–11]; however, they are not optically transparent. PGs are also widely used in optoelectronics and biomedicine due to their wide optical transmission window, high composition flexibility, and high solubility of rare-earth ions for laser applications [6,17–20]. Nonetheless, these types of phosphate optical glasses are not bioresorbable (i.e., one that dissolves in a biological fluid).

In previous studies, Ceci-Ginistrelli et al. proposed a calcium-phosphate glass formulation that was drawable in the form of fiber and optically transparent from the ultraviolet (UV) to the near-infrared (NIR) [21]. This success was attained by carefully selecting glass-making reagents to produce a bioresorbable material that could be cast in a fiber preform and then drawn as an optical fiber using the rod-in-tube technique [21]. The most promising features of bioresorbable optical device implants are the potential reduction of medical costs and the complexity of diagnosis and therapy procedures since there is no need to have post-insertion procedures to remove the implant [22]. Applications of those fibers can cover: deep-tissue photodynamic therapy (PDT) [23], gas and liquid sensing [19,24,25], and in vivo imaging [20]. In particular, in vivo studies for the biological response of phosphate-based optical fibers have shown to have no adverse effect on animals [20].

The mechanical behavior of PG fibers has been investigated both as core/cladding fibers and as capillaries [6]. Hole drilling is one of the conventional methods of fabricating capillaries. Although PG exhibits good mechanical properties, fabricating microstructured optical fibers and capillaries using conventional hole drilling techniques is time-consuming and has high equipment costs (i.e., ultrasonic drilling). Furthermore, it is limited to a small number of holes [26]. Another method for fabricating capillaries is rotational casting. However, there are two main disadvantages to this method. First, the outer and inner roughness of the surface could be high, and the overall surface quality can raise quality concerns in the drawing process. Second, the preform and produced fiber shape is cylindrical, and its inner-to-outer diameter ratio is limited to at most $0.4 \div 0.6$ [6,19,27].

Another conventional technique to shape a variety of materials is extrusion. It entails driving a suitably soft material (e.g., heated alloy, heated glass, or polymer sample) through an aperture, namely a die, to get it to a defined shape. After passing through the die, the softened material is cooled to a temperature below its glass transition temperature, maintaining the imposed shape. Extrusion is arguably the most suitable method where objects with a fixed cross-sectional profile are required [27]. Studies on the extrusion of glass materials date back to the early 1970s [28]; however, since the hole drilling technique results on silicate-based glasses were reasonable, the studies on the extrusion of glasses were seldom studied [28]. Recently, more studies on different glasses such as phosphate, lead silicate, tellurite, bismuth, and fluoride glass with particular use as optical fibers have been conducted. As a result of these studies, extrusion was used again to fabricate rods, capillaries, cores and claddings, and even microstructured fibers [14,22,29–42]. Although these studies significantly improved the extrusion process, die design, and extrudate shape, nevertheless, some areas require more investigation. One of the most persisting issues up to recently is

preform distortion due to a lack of a quick and straightforward approach for quickly determining the primary design characteristics that would allow for intelligent die design.

Gallichi-Nottiani et al. recently proposed that a quick optimization cycle is preferable to a more complicated and rigorous mathematical model [27]. That study exploited a Computational Fluid Dynamics (CFD) approach to dig deeper into the die design and parameters, especially for extrusion of more complex shapes like the double hole and microstructured preforms [27]. Combining the bioresorbablity of phosphate glass with the optical transparency of optical fibers creates new possibilities in the diagnosis and therapy of patients. In our group's previous investigations, Ceci-Ginistrelli et al. fabricated PG capillaries and investigated mechanical, optical, and in vitro properties [21,43]. In the above-mentioned study, Gallichi-Nottiani et al. targeted a PG microstructured optical fiber using extrusion combined with the stack-and-draw technique with successful results [27]. Although previous studies have provided a comprehensive understanding of phosphate glass extrusion, it is still necessary to investigate the methods of fabricating preforms with low bending and tapering. These preforms could effectively be used for rod-in-tube and stack-and-draw techniques, allowing to obtain more complex microstructures that incorporate multiple functionalities.

This study proposes a method to fabricate a microstructured fiber with a capillary hole and a multimode core. Direct extrusion, stack-and-draw and rod-in-tube techniques were used to fabricate the preform, which was then drawn to manufacture the final optical fiber. This fiber consists of one capillary section to deliver liquid material by surface tension force and one core/cladding section to guide light throughout the fiber. Finally, the main characteristics of this optical fiber are reported and discussed.

2. Materials and methods

2.1 Glass fabrication

Bioresorbable PG samples were fabricated using two slightly different compositions. The core and the cladding have a difference in refractive index for efficient light guiding within the core part of the microstructured fiber. For the cladding and capillary, the composition (in mol%) is 50 P_2O_5 – 23 MgO – 11.5 Na_2O – 10 CaO – 3 SiO_2 – 2.5 B_2O_3, herein PG1, and the core composition (in mol%) is 50 P_2O_5 – 3 MgO – 11.5 Na_2O – 30 CaO – 3 SiO_2 – 2.5 B_2O_3, herein PG2. These compositions were derived from previous studies [6,21,27]. The high amount of MgO lowers the refractive index while increasing the elastic modulus of the fiber [6]. High purity (>99%) oxide reagents were weighed and mixed in a dry box to minimize the hydroxyl ions (OH^-) content in the final glass. The conventional melt-quenching technique was used to prepare glass samples. The powder mixture was melted at 1200 °C for 2 h inside a furnace with dry air flux, and then the molten glass was cast into a preheated stainless steel mold. The annealing procedure immediately began at a temperature close to glass transition temperature (T_g) for 5 h. The sample then cooled down slowly to room temperature. The obtained glass billet weighed around 45 g and had a diameter of 25 mm, and a height of 30 to 35 mm. The bioresorbability of these glass compositions in fiber form

was tested in phosphate-buffered saline (PBS) solution by Ceci-Ginistelli et al.'s protocols [21].

2.1 Glass characterization

The refractive index of the glass was measured at 633 nm wavelength using a Metricon 2010 Prism Coupler. In the previous study of this group, Gallichi-Nottiani et al. used a thermo-mechanical analyzer (TMA, model SETARAM—SETSYS Evolution) to assess the bioresorbable glass viscosity [27]. They used ASTM Standard C1351M-96 to compute the glass viscosity [27]. In the previous study of this group, glass density was measured at room temperature by Archimedes' method [21]. Also, differential thermal analysis (DTA) by Netzsch DTA 404 PC was performed to measure the characteristic temperatures of manufactured glasses.

2.3 Extrusion

The extrusion system employed in this study is home-built. It consists of the following components: (i) the driving motor (brushless DC motor), (ii) an electrically heated furnace, (iii) a thermocouple that is in contact with the die base to constantly monitor the furnace temperature, (iv) the stainless steel ram connected to the motor, (v) a holding Inconel (Nickel-based alloy) cylinder used to support (vi) the die (made of AISI 304 stainless steel), (vii) the glass billet that will go inside the Inconel cylinder. The applied force is controlled by (viii) a load cell placed between the ram and the motor. The extrusion force is ranged from 100 to 5000 N, which is dependent on the die design and glass characteristics. The average value used in this experiment is 600 N. Three tubes were fabricated with different inner and outer diameters to use the stack-and-draw technique. The first die has 4.5 mm pin and 10 mm outer diameter, and the second and third tubes are made from the 7 mm pin and 10 mm outer diameter die.

2.4 Microstructured fiber drawing

Cylindrical preforms were fabricated with the help of dies with dimensions of 10 mm outer diameter (OD) and 4.5 and 7.4 mm pins. Preform with a smaller inner diameter (ID) is used as a cladding for the core-cladding fiber. PG2 with a higher refractive index is used as a core, and this core/cladding preform stretched to the desired diameter. Other preform tubes with 6.7 mm inner and 10 mm outer diameters are used for stretching as capillaries and the outer cladding of the double hole fiber. Stretched rods with a diameter of 0.5, 0.7 and 0.8 mm were fabricated with the same PG1 as the cladding and capillary, and used as fillers. Preform assembly was performed in a controlled atmosphere to minimize contamination. Figure 1 illustrates the preform assembly process. The bundle consists of one core/cladding tube with a 2.2 mm diameter, one capillary tube with 1.05 mm ID and 3.3 mm OD, and several 0.5 mm, 0.7, and 0.8 mm rods as fillers. They are all inserted into the outer tube with a 6.7 mm hole. Finally, the preform was processed in an in-house constructed drawing tower. An induction heating ring running at 248 kHz with 170 W power (SAET, Torino, Italy) was used to reach the drawing temperature. The drawing tower settings were selected to draw 130 to 230 μm diameter fibers, which corresponds to the typical range of the fiber dimensions used for telecom, optics, and biomedical applications.

2.5 Fiber characterization

Some of the broken fiber samples cross-sections, previously coated with a thin sputtered layer of Au-Pd, were analyzed with Scanning Electron Microscope (SEM) (ZEISS, Supra, Germany). The cut-back approach assessed fiber losses at 1300 nm using a single-mode fiber pigtailed laser diode source (Infineon SBM 52414x). The laser was end face coupled to one of the cleaved active fiber ends. The attenuation value was derived by fitting the experimental data with linear least squares. The optical fiber's modal properties were examined by obtaining a series of near-field photographs of the fiber cross-section at 1300 nm wavelengths with butt-coupled fiber pigtailed laser diode sources. The liquid delivery in the microchannel was realized by coupling 30 cm of fiber to a syringe and sealing the junction of the fiber with the syringe with cyanoacrylate glue. The colored liquid was realized by a solution of Methylene Blue with deionized water with a 100 μM concentration. The evolution of the delivery of the liquid in the capillary was recorded under a microscope with a transmission illumination and a 10X objective.

3. Results and discussion

3.1 Bioresorbable optical fiber

Optical fiber fabrication consists of several steps, from glass production to the final drawing. In our study, the first step is glass billet fabrication, which must be done carefully under a controlled atmosphere in the glove box to avoid any contamination and OH- group that causes high optical loss. The second step is to extrude the glass billets into the desired shape and size to prepare rods and tubes. The third step is preparing the optical fiber preform by the stack-and-draw technique. This technique consists in filling a glass tube with glass rods, capillary, and fillers to draw a microstructured fiber capable of guiding light and liquid simultaneously. If one of these steps has any flaws, the final fiber could suffer from defects such as air bubbles inside the fiber or crystallization of the glass, which affect the attenuation loss of the fiber.

We carried out several studies to obtain an almost defect-free glass preform. It is needed to realize the best composition and procedure to cast a perfect glass free from tiny air bubbles and showing a low surface roughness with no residual stress. Details about the phosphate glass's composition and physical and optical properties are presented in Ceci-Ginistrelli et al. [21]. This glass has a wide optical window from 240 to 2500 nm, from the UV edge toward NIR wavelengths, with no absorption peaks [21].

Two bioresorbable phosphate glasses with slightly different compositions were made to obtain the waveguiding effect of a core/cladding structure. A slight difference in MgO content leads to a different refractive index required to have total internal reflection (TIR) phenomena that lead to guiding light through the core-cladding section of the final fiber. The glasses' composition, optical, and physical properties are shown in Table 1. This bioresorbable glass contains 50 mol% of P2O5. This amount of P2O5 makes the glass easier to draw by forming a polymeric-like network [45]. After melting the glass in the furnace and keeping it for a few hours, the molten glass was cast into a cylindrical mold to form a billet about 40 mm in height and 25 mm in diameter. These billets were used for the extrusion of tubes.

Table 1. Properties of phosphate glasses used as the core, cladding, and capillary: MgO content in mol%, glass density ρ, glass transition temperature Tg, onset crystallization temperature Tx, working

temperature range ΔT (i.e., the difference between onset crystallization and glass transition temperatures), transparency window TW, and refractive index n measured at a wavelength of 633 nm. ([a]Data from [27], [b]Data from [21]).

	MgO **[mol%]**	ρ **[g/cm^3]** [a]	T_g **[°C]**[a]	T_x **[°C]** [a]	ΔT **[°C]** [a]	***TW*** **[nm]**[b]	***n***
		± 0.005	± 3	± 3	± 6	÷ 2500	± 0.001
PG1	23	2.589	477	625	148	240	1.515
PG2	3	2.606	435	658	223	240	1.527

3.2 Extrusion, assembly, and fiber drawing

A perfect extrudate is free from stains, tiny air bubbles, and crystals and has a low surface roughness. In terms of shape, it has almost no tapering, bending, or swelling, and it has a sufficient length to make fiber drawing possible. In practice, it is hard to fabricate such a sample, but keeping above mentioned flaws as low as possible contributes to a performing optical fiber.

Gallichi-Nottiani et al. made a viscosity measurement from melt-quenched glass. They found that the reference working temperature for the glass extrusion is 517 to 552 °C, which corresponds to viscosities from 10^8 to $10^{6.5}$ Pa·s [27]. As shown in Table 1, the working temperature of the glass that is the difference between T_x and T_g is 148 °C, which makes extrusion and fiber drawing possible without any chance for recrystallization.

Heike Ebendorff-Heidepriem et al. investigated the effect of materials used for die fabrication on the glass flow, pointing out the difference between stainless steel dies and graphite dies [40]. The study concluded that graphite dies exhibited non-wetting behavior, resulting in a fluid slip at the glass/die boundary, which significantly reduced friction for glass flow within the die. Whereas stainless steel dies were indicated to follow the Poiseuille's equation for fluid flow, the pressure required to extrude a glass through a die is proportional to the volume flow rate and glass viscosity [40]. Another study by the same group discovered that the taper decreases with increasing speed and decreasing temperature. Since the glass is hanging under its weight at higher speeds for a shorter time and at lower temperatures, the glass is in a more viscous state during the period it is hanging from the lower part of the die channel. Subsequently, increasing speed and reducing the temperature during extrusion leads to the higher force needed for extrusion [46].

Gallichi-Nottiani et al. also studied the effect of temperature, force, and die geometry on the phosphate glass extrudate using Computational Fluid Dynamics (CFD) and confirmed it with experimental data from various extrusions [27]. In the mentioned work, extrusion of the tubes was done at 540 °C, equivalent to nominal viscosity of 10^7 Pa·s, with a force of 800 N and ram speed of about 120 μm/min [27]. These data were used as a starting point to make extrudate with lower and more negligible initial bending, overall bending, and tapering.

After several experiments, we found that the best parameters for extruding are as follows: 535 °C temperature ($10^{7.2}$ Pa·s viscosity), 900 N force, and about 200 μm/min ram speed. At such temperature, the viscosity is low enough to make glass flow under pressure and high enough to be solid right after the die. In this manner, the extrudate's weight does

not significantly affect the tapering. Thus, tapering is reduced by increasing the speed of the ram and lowering the temperature. This procedure also leads to low outer diameter swelling. Indeed, this leads to an extrudate with at most 1.8 and 3.5 µm/mm outer and inner tapering, respectively, achieving a final length of 280 mm.

Three glass tubes with different ID and OD were used for different optical fiber parts. Table 2 summarizes the geometry and procedure of each part of the glass used to fabricate the final microstructured fiber. Extrudate dimension from the die with a pin diameter of 7.40 mm and die diameter of 10.15 mm was about ID = 6.70 mm, and OD = 10.20 mm outer diameter. The same goes for the 5.25 mm – 10.50 mm (pin and outer diameter, respectively) die, with ID = 4.45 mm and OD = 10.40 mm extrudate dimensions. These results indicate a 10% reduction and 0.4% increase for ID/Pin and OD/Die ratio for the (7.4 mm – 10 mm) die. Also, a 15 and 1% reduction in ID/Pin and OD/Die ratio for the (4.5 mm – 10 mm) die. These results align with Kalnins et al. with noticeable improvements [46].

Table 2. Glass preforms geometry, fabrication methods, and the roles in the final optical fiber.

Glass name	**Glass role**	**OD [mm]**	**ID [mm]**	**Fabrication method**
PG1	Outer tube	10.20	5.80	Extrusion
PG1	Capillary	3.30	1.05	Extrusion + stretching
PG1	Cladding	2.20	0.83	Extrusion + stretching
PG2	Core	0.83	-	Cast + stretching
PG1	Fillers	0.50 - 0.73 - 0.83	-	Cast + stretching

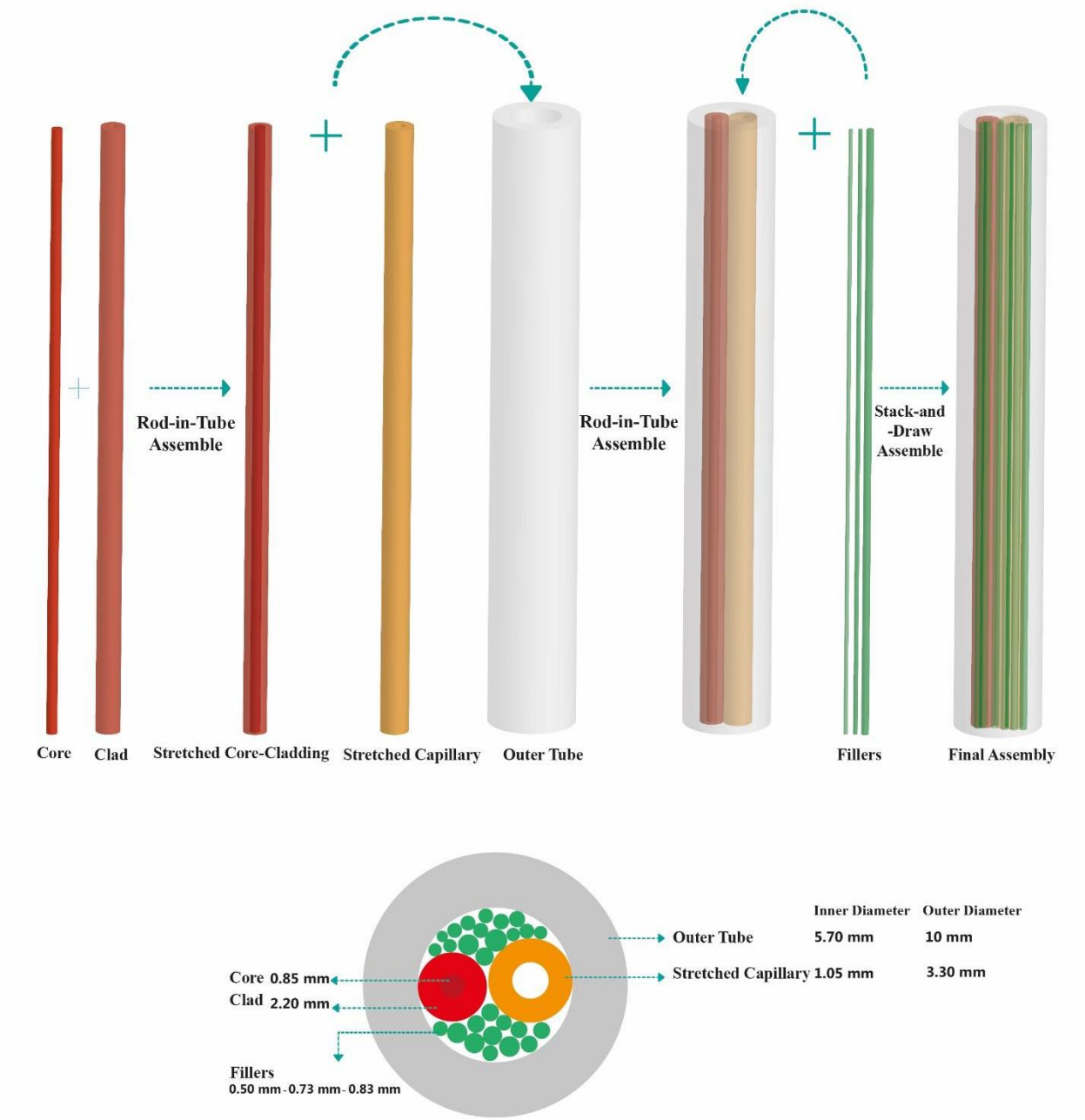

Fig. 1. Fabrication, assembly and sizes of core-cladding, capillary and fillers, using multistage rod-in-tube and stack-and-draw techniques. Graphics are in color for better visualization.

To assemble the preform, the strategy employed for the stack-and-draw is illustrated in the schematics of Figure 1. The first step is to put the cast and polished PG2 rod with 4.3 mm diameter inside the preform with 4.45 mm ID and 10 mm OD, by utilizing the rod-in-tube technique and stretching it in the drawing tower to form a core-cladding glass. As mentioned before, the refractive index of PG2 has a slight difference from PG1 (cladding) to have a TIR effect and thus guide light through the final optical fiber.

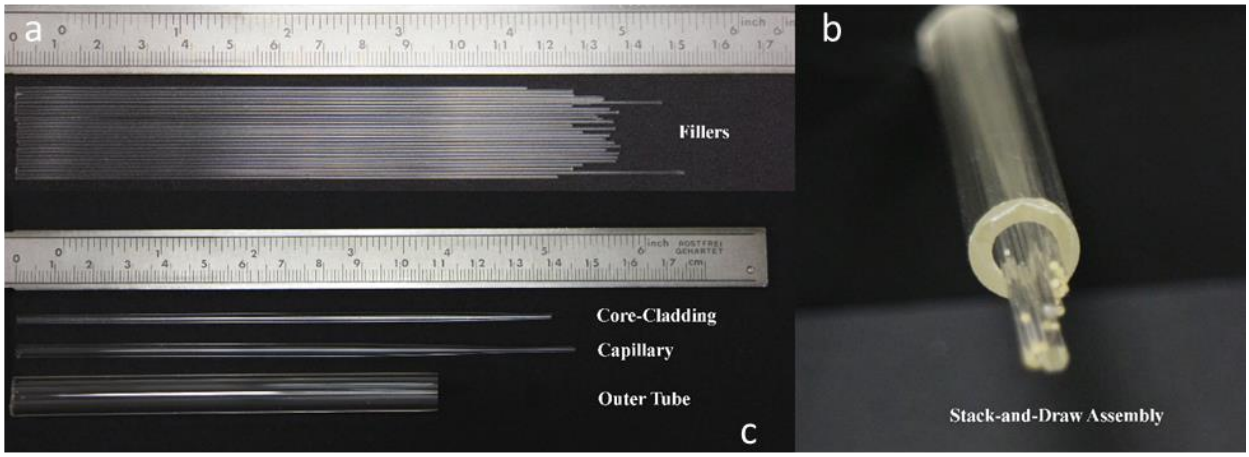

Fig. 2. Different parts of the final preforms assembly: (a) Fillers, (b) from top to down: core-cladding, capillary, and outer tube. (c) components stacked inside the outer tube.

The core cladding rod-in-tube was stretched to obtain the light guiding part of the preform. The following step towards the final preform assembly is the realization of a capillary that could be used either as the outer tube or as a filler tube if properly collapsed. To obtain the filler rods a cast PG1 glass rod was stretched to different diameters (0.50, 0.73, and 0.83 mm diameters). All the stretched tube elements (core-cladding, capillary, and filler) were inserted inside the outer tube made from PG1 (i.e., a glass tube with about 5.8 mm ID and 10.1 OD).

The sizes of fillers used to fill all the gaps inside the outer shell are differentiated to obtain an easier filling between the core-cladding and the capillary void elements. Since the fillers' diameters are less than 1 mm, it is easy to break them during the insertion inside the tube. This issue is one of the drawbacks of this assembly method compared to a direct two-hole preform extrusion. On the other hand, it is a more flexible approach that allow to easily change the dimension of the core-cladding and capillaries to the requirements of the experiment in this method by adjusting the stretching, whereas changing sizes in extrusion requires new dies and further process optimization, making the last approach expensive and time-consuming. Another critical aspect of the stack and draw from extruded tubes is represented by the fact that a slight bending, distortion, or tapering in the preforms might severely affect the rod-in-tube assembly. Although, by leveraging the straight tube from the optimized extrusion process, this issue was greatly reduced. Indeed, in Figure 2 are presented all the elements of the preform: the outer shell, stretched tubes, and rods as fillers. Even in the final stack-and-draw assembly, the transparency and straightness of the preforms are noticeable. As shown in Figure 2c, the final preform was realized and then mounted in the drawing tower to fabricate the fiber batches. Using an RF induction heating system, the preforms were drawn to fibers at around 550 °C under a controlled nitrogen atmosphere. By changing the drawing conditions, two microstructured fibers were produced with 130 and 230 μm diameter and capillary diameter sizes of 17 and 25 μm, respectively.

3.3 Characterization

SEM and optical microscopy were used to visualize the fiber cross-section. Figure 3a and b show a cross-section of 230 µm fiber under the electron and optical microscopes, respectively, where both the core and the channel are visible. The optical fiber output was characterized by a camera (Xeva XC 130 Camera) by injecting the core with a diode laser at 1300 nm. An objective lens was utilized to make an image from a cross-section of 80 cm length of the 130 µm diameter microstructured fiber and to examine the light-guiding performance. Figure 3c shows that the light is well confined into the core.

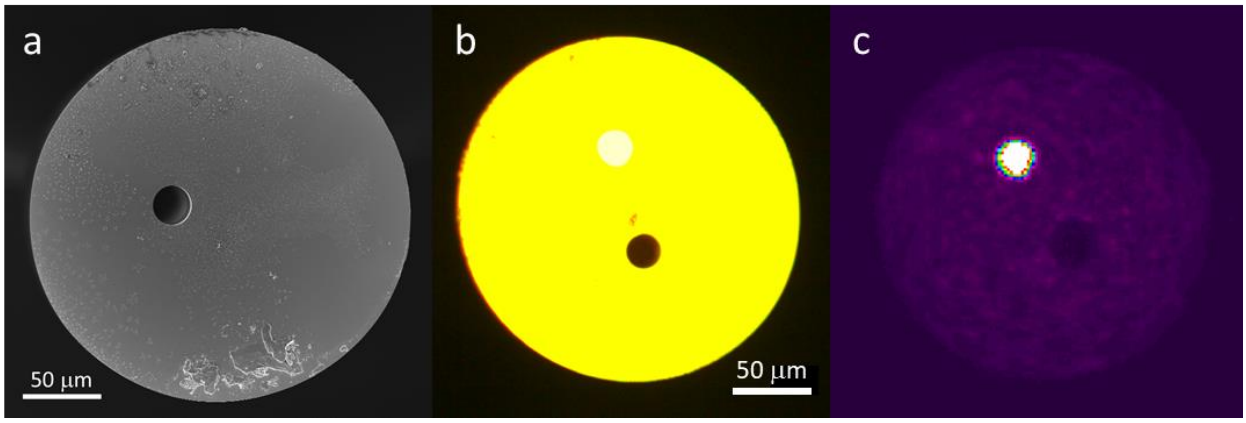

Fig. 3. a) SEM image of the facet of the fiber of 230 µm diameter; b) microscope image of its facet, and c) optical fiber output of guided light at 1300nm.

The optical loss of the multimode core/cladding fiber is measured at 1300 nm and is estimated to be 2.4 dB/m. These results are consistent with previous studies on the same glass optical fiber [21]. Mechanical properties of the bioresobable fiber have been investigated by Sglavo et al. and the elastic modulus and tensile strength, are reported in Table 3 for the sake of completeness.

Table 3. Elastic modulus (E) [GPa] and tensile strength (σF) [MPa] of the fiber (Sglavo et al. 2019).

Glass Role	**Glass name**	***E* [GPa]**	**σ_F [MPa]**
Optical fiber	PG2/PG1	51.1 ± 0.9	366
Core capillary	PG2	48.3 ± 0.6	276
Cladding capillary	PG1	53.1 ± 0.2	359

The bioresorbability of the fibers from this glass system was studied in another study of our group using PBS solution at pH = 7.4 and a temperature of 37 °C. Solution volume/sample exposed area was 0.1 ml/mm2. The result was 37% weight loss in 21 days for the PG1 [21].

To demonstrate the capability of liquid delivery, a setup was created by injecting colored water into the 200 mm fiber with a 230 µm diameter to examine how the liquid flows inside the 25 µm capillary hole. In figure 4, the liquid flow inside the capillary is visible demonstrating the liquid delivery functionality of the microstructured fiber. This type of microfluidic channel is comparable to standard planar channels and allow for a flow of around 10-50µl/min which is compatible with the release of drugs or staining agents.

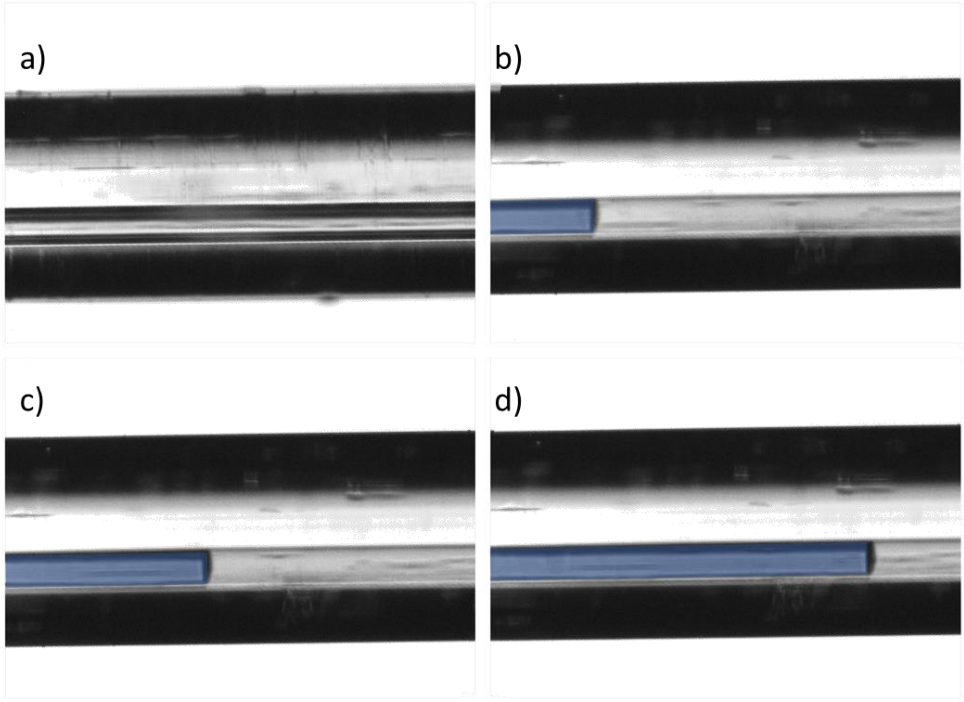

Fig. 4. Microscope image at 10X of the capillary hole inside the fiber starting from (a) empty and gradually filled (b,c,d) with colored water demonstrating the fluid flow inside the fiber.

4. Conclusions

This study presents a microstructured bioresorbable optical fiber comprising a multimode core and a microfluidic channel in the same fiber. The study encompasses two slightly different glass compositions used as core-cladding parts. Casting and extrusion parameters are optimized to achieve straight extrudate with minimum tapering. Glass preforms are made with casting billets and extrusion, then stretched to the desired dimensions. Rod-in-tube technique is used to make the core-cladding part. Stretching casted glass to fillers made all the components of the final stack-and-draw assembly possible. This assembly is drawn to 130 and 230 µm diameter fibers. Optical microscopy is used to visualize the light guiding capability of the core-cladding fiber. Light confinement was examined by a Xeva camera coupled with a laser. The corresponding images show that light is well confined in the core. Also, the attenuation loss of the optical fiber at 1300 nm was measured to be 2.4 dB/m, which is consistent with the previous study. A setup consisting of colored liquid was used to examine the capillary performance of delivering liquid and a

demonstration with flow of methylene blue was performed. This novel fiber could contribute significantly to the biomedical field, especially theranostics applications where the ability to delivery liquids and light at the same time could enable advanced biophotonics configuration with fibers implanted in the human body.

Acknowledgements

The authors acknowledge support from the interdepartmental center PhotoNext, and LINKS foundation.

References

[1] F. Baino, S. Hamzehlou, S. Kargozar, Bioactive glasses: Where are we and where are we going?, J. Funct. Biomater. 9 (2018). https://doi.org/10.3390/jfb9010025.

[2] A. Baranowski, A. Klein, U. Ritz, H. Götz, S.G. Mattyasovszky, P.M. Rommens, A. Hofmann, Evaluation of bone sialoprotein coating of three-dimensional printed calcium phosphate scaffolds in a calvarial defect model in mice, Materials (Basel). 11 (2018). https://doi.org/10.3390/ma11112336.

[3] T. Ahlfeld, A.R. Akkineni, Y. Förster, T. Köhler, S. Knaack, M. Gelinsky, A. Lode, Design and Fabrication of Complex Scaffolds for Bone Defect Healing: Combined 3D Plotting of a Calcium Phosphate Cement and a Growth Factor-Loaded Hydrogel, Ann. Biomed. Eng. 45 (2017) 224–236. https://doi.org/10.1007/s10439-016-1685-4.

[4] S.J. H, B.S. M, Calcium phosphate scaffolds for bone repair, Jom. (2011) 83–92.

[5] H. Sun, C. Hu, C. Zhou, L. Wu, J. Sun, X. Zhou, F. Xing, C. Long, Q. Kong, J. Liang, Y. Fan, X. Zhang, 3D printing of calcium phosphate scaffolds with controlled release of antibacterial functions for jaw bone repair, Mater. Des. 189 (2020) 108540. https://doi.org/10.1016/j.matdes.2020.108540.

[6] V.M. Sglavo, D. Pugliese, F. Sartori, N.G. Boetti, E. Ceci-Ginistrelli, G. Franco, D. Milanese, Mechanical properties of resorbable calcium-phosphate glass optical fiber and capillaries, J. Alloys Compd. 778 (2019) 410–417. https://doi.org/10.1016/j.jallcom.2018.11.033.

[7] A. Barba, A. Diez-Escudero, Y. Maazouz, K. Rappe, M. Espanol, E.B. Montufar, M. Bonany, J.M. Sadowska, J. Guillem-Marti, C. Öhman-Mägi, C. Persson, M.C. Manzanares, J. Franch, M.P. Ginebra, Osteoinduction by Foamed and 3D-Printed Calcium Phosphate Scaffolds: Effect of Nanostructure and Pore Architecture, ACS Appl. Mater. Interfaces. 9 (2017) 41722–41736. https://doi.org/10.1021/acsami.7b14175.

[8] C.J.D. Bergmann, J.C.E. Odekerken, T.J.M. Welting, F. Jungwirth, D. Devine, L. Bouré, S. Zeiter, L.W. Van Rhijn, R. Telle, H. Fischer, P.J. Emans, Calcium phosphate based three-dimensional cold plotted bone scaffolds for critical size bone defects, Biomed Res. Int. 2014 (2014). https://doi.org/10.1155/2014/852610.

[9] A.G. Dias, M.A. Lopes, J.D. Santos, A. Afonso, K. Tsuru, A. Osaka, S. Hayakawa, S. Takashima, Y. Kurabayashi, In vivo performance of biodegradable calcium phosphate glass ceramics using the rabbit model: Histological and SEM observation, J. Biomater. Appl. 20 (2006) 253–266. https://doi.org/10.1177/0885328206052466.

[10] M. Schumacher, L. Reither, J. Thomas, M. Kampschulte, U. Gbureck, A. Lode, M. Gelinsky, Calcium phosphate bone cement/mesoporous bioactive glass composites for controlled growth factor delivery, Biomater. Sci. 5 (2017) 578–588. https://doi.org/10.1039/c6bm00903d.

[11] S. Etter, F. Despetis, P. Etienne, Sub-critical crack growth in some phosphate glasses, J. Non. Cryst. Solids. 354 (2008) 580–586. https://doi.org/10.1016/j.jnoncrysol.2007.07.093.

[12] A.J. Parsons, I. Ahmed, P. Haque, B. Fitzpatrick, M.I.K. Niazi, G.S. Walker, C.D. Rudd, Phosphate

Glass Fibre Composites for Bone Repair, J. Bionic Eng. 6 (2009) 318–323. https://doi.org/10.1016/S1672-6529(08)60132-8.
[13] M. Bohner, G. Baroud, Injectability of calcium phosphate pastes, Biomaterials. 26 (2005) 1553–1563. https://doi.org/10.1016/j.biomaterials.2004.05.010.
[14] N. Sharmin, A.J. Parsons, C.D. Rudd, I. Ahmed, Effect of boron oxide addition on fibre drawing, mechanical properties and dissolution behaviour of phosphate-based glass fibres with fixed 40, 45 and 50 mol% P2O5, J. Biomater. Appl. 29 (2014) 639–653. https://doi.org/10.1177/0885328214539824.
[15] S. Samavedi, A.R. Whittington, A.S. Goldstein, Calcium phosphate ceramics in bone tissue engineering: A review of properties and their influence on cell behavior, Acta Biomater. 9 (2013) 8037–8045. https://doi.org/10.1016/j.actbio.2013.06.014.
[16] H. Guo, J. Wei, Y. Yuan, C. Liu, Development of calcium silicate/calcium phosphate cement for bone regeneration, Biomed. Mater. 2 (2007) S153–S159. https://doi.org/10.1088/1748-6041/2/3/S13.
[17] D. Pugliese, M. Konstantaki, I. Konidakis, E. Ceci-Ginistrelli, N.G. Boetti, D. Milanese, S. Pissadakis, Bioresorbable optical fiber Bragg gratings, Opt. Lett. 43 (2018) 671. https://doi.org/10.1364/ol.43.000671.
[18] J. Massera, Y. Shpotyuk, F. Sabatier, T. Jouan, C. Boussard-Plédel, C. Roiland, B. Bureau, L. Petit, N.G. Boetti, D. Milanese, L. Hupa, Processing and characterization of novel borophosphate glasses and fibers for medical applications, J. Non. Cryst. Solids. 425 (2015) 52–60. https://doi.org/10.1016/j.jnoncrysol.2015.05.028.
[19] P. Lopez-Iscoa, N. Ojha, D. Pugliese, A. Mishra, R. Gumenyuk, N.G. Boetti, D. Janner, J. Troles, B. Bureau, C. Boussard-Plédel, J. Massera, D. Milanese, L. Petit, Design, processing, and characterization of an optical core-bioactive clad phosphate fiber for biomedical applications, J. Am. Ceram. Soc. 102 (2019) 6882–6892. https://doi.org/10.1111/jace.16553.
[20] O. Podrazký, P. Peterka, I. Kašík, S. Vytykáčová, J. Proboštová, J. Mrázek, M. Kuneš, V. Závalová, V. Radochová, O. Lyutakov, E. Ceci-Ginistrelli, D. Pugliese, N.G. Boetti, D. Janner, D. Milanese, In vivo testing of a bioresorbable phosphate-based optical fiber, J. Biophotonics. 12 (2019). https://doi.org/10.1002/jbio.201800397.
[21] E. Ceci-Ginistrelli, D. Pugliese, N.G. Boetti, G. Novajra, A. Ambrosone, J. Lousteau, C. Vitale-Brovarone, S. Abrate, D. Milanese, Novel biocompatible and resorbable UV-transparent phosphate glass based optical fiber, Opt. Mater. Express. 6 (2016) 2040. https://doi.org/10.1364/ome.6.002040.
[22] C.A.G. Kalnins, N.A. Spooner, T.M. Monro, H. Ebendorff-Heidepriem, E. Bailey, Surface Analysis and Treatment of Extruded Fluoride Phosphate Glass Preforms for Optical Fiber Fabrication, J. Am. Ceram. Soc. 99 (2016) 1874–1877. https://doi.org/10.1111/jace.14269.
[23] T.J. Dougherty, C.J. Gomer, B.W. Henderson, G. Jori, D. Kessel, M. Korbelik, J. Moan, Q. Peng, Photodynamic therapy, J. Natl. Cancer Inst. 90 (1998) 889–905. https://doi.org/10.1093/jnci/90.12.889.
[24] A.M. Cubillas, S. Unterkofler, T.G. Euser, B.J.M. Etzold, A.C. Jones, P.J. Sadler, P. Wasserscheid, P.S.J. Russell, Photonic crystal fibres for chemical sensing and photochemistry, Chem. Soc. Rev. 42 (2013) 8629–8648. https://doi.org/10.1039/c3cs60128e.
[25] R. Nazempour, Q. Zhang, R. Fu, X. Sheng, Biocompatible and implantable optical fibers and waveguides for biomedicine, Materials (Basel). 11 (2018). https://doi.org/10.3390/ma11081283.
[26] X. Feng, A.K. Mairaj, D.W. Hewak, T.M. Monro, Nonsilica glasses for holey fibers, J. Light. Technol. 23 (2005) 2046–2054. https://doi.org/10.1109/JLT.2005.849945.
[27] D. Gallichi-Nottiani, D. Pugliese, N. Giovanna Boetti, D. Milanese, D. Janner, Toward the fabrication of extruded microstructured bioresorbable phosphate glass optical fibers, Int. J. Appl. Glas. Sci. 11 (2020) 632–640. https://doi.org/10.1111/ijag.14652.

[28] E. Roeder, Extrusion of glass, J. Non. Cryst. Solids. 5 (1971) 377–388. https://doi.org/10.1016/0022-3093(71)90039-1.
[29] S.C. Warren-Smith, A. Dowler, H. Ebendorff-Heidepriem, Soft-glass imaging microstructured optical fibers, Opt. Express. 26 (2018) 33604. https://doi.org/10.1364/oe.26.033604.
[30] M. Zhu, X. Wang, Z. Pan, C. Cheng, Q. Zhu, C. Jiang, Q. Nie, P. Zhang, Y. Wu, S. Dai, T. Xu, G. Tao, X. Zhang, Fabrication of an IR hollow-core Bragg fiber based on chalcogenide glass extrusion, Appl. Phys. A Mater. Sci. Process. 119 (2015) 455–460. https://doi.org/10.1007/s00339-015-9017-3.
[31] X. Xiao, Y. Xu, J. Cui, X. Liu, X. Cui, X. Wang, S. Dai, H. Guo, Structured active fiber fabrication and characterization of a chemically high-purified Dy3+-doped chalcogenide glass, J. Am. Ceram. Soc. 103 (2020) 2432–2442. https://doi.org/10.1111/jace.16921.
[32] R.R. Gattass, D. Rhonehouse, D. Gibson, C.C. McClain, R. Thapa, V.Q. Nguyen, S.S. Bayya, R.J. Weiblen, C.R. Menyuk, L.B. Shaw, J.S. Sanghera, Infrared glass-based negative-curvature anti-resonant fibers fabricated through extrusion, Opt. Express. 24 (2016) 25697. https://doi.org/10.1364/oe.24.025697.
[33] M. Trabelssi, P.F. Joseph, Hole distortion and drift in extruded microstructured optical fiber glass preforms: Part I – Sensitivity analysis, J. Non. Cryst. Solids. 481 (2018) 412–423. https://doi.org/10.1016/j.jnoncrysol.2017.10.045.
[34] H. Ebendorff-Heidepriem, S.C. Warren-Smith, T.M. Monro, Suspended nanowires: fabrication, design and characterization of fibers with nanoscale cores, Opt. Express. 17 (2009) 2646. https://doi.org/10.1364/oe.17.002646.
[35] M. Trabelssi, H. Ebendorff-Heidepriem, K.A. Richardson, T.M. Monro, P.F. Joseph, Computational modeling of hole distortion in extruded microstructured optical fiber glass preforms, J. Light. Technol. 33 (2015) 424–431. https://doi.org/10.1109/JLT.2015.2388733.
[36] H. Ebendorff-Heidepriem, T.-C. Foo, R.C. Moore, W. Zhang, Y. Li, T.M. Monro, A. Hemming, D.G. Lancaster, Fluoride glass microstructured optical fiber with large mode area and mid-infrared transmission, Opt. Lett. 33 (2008) 2861. https://doi.org/10.1364/ol.33.002861.
[37] X. Feng, F. Poletti, A. Camerlingo, F. Parmigiani, P. Horak, P. Petropoulos, W.H. Loh, D.J. Richardson, Dispersion-shifted all-solid high index-contrast microstructured optical fiber for nonlinear applications at 155μm, Opt. Express. 17 (2009) 20249. https://doi.org/10.1364/oe.17.020249.
[38] H. Ebendorff-Heidepriem, T.M. Monro, Extrusion of complex preforms for microstructured optical fibers, Opt. Express. 15 (2007) 15086. https://doi.org/10.1364/oe.15.015086.
[39] A. Belwalkar, H. Xiao, W.Z. Misiolek, J. Toulouse, Extruded tellurite glass optical fiber preforms, J. Mater. Process. Technol. 210 (2010) 2016–2022. https://doi.org/10.1016/j.jmatprotec.2010.07.018.
[40] H. Ebendorff-Heidepriem, T.M. Monro, Analysis of glass flow during extrusion of optical fiber preforms, Opt. Mater. Express. 2 (2012) 304. https://doi.org/10.1364/ome.2.000304.
[41] G. Tsiminis, K.J. Rowland, E.P. Schartner, N.A. Spooner, T.M. Monro, H. Ebendorff-Heidepriem, Single-ring hollow core optical fibers made by glass billet extrusion for Raman sensing, Opt. Express. 24 (2016) 5911. https://doi.org/10.1364/oe.24.005911.
[42] Z.G. Lian, Q.Q. Li, D. Furniss, T.M. Benson, A.B. Seddon, Solid microstructured chalcogenide glass optical fibers for the near- and mid-infrared spectral regions, IEEE Photonics Technol. Lett. 21 (2009) 1804–1806. https://doi.org/10.1109/LPT.2009.2033208.
[43] E. Ceci-Ginistrelli, C. Pontremoli, D. Pugliese, N. Barbero, N.G. Boetti, C. Barolo, S. Visentin, D. Milanese, Drug release kinetics from biodegradable UV-transparent hollow calcium-phosphate glass fibers, Mater. Lett. 191 (2017) 116–118. https://doi.org/10.1016/j.matlet.2016.12.103.
[44] ASTM:C1557-14, Standard Test Method for Tensile Strength and Young's Modulus of Fibers, (2016) 1–10. https://www.astm.org/c1557-20.html (accessed April 6, 2022).

[45] J.C. Knowles, Phosphate based glasses for biomedical applications, J. Mater. Chem. 13 (2003) 2395–2401. https://doi.org/10.1039/b307119g.
[46] C.A.G. Kalnins, K.J. Bachus, A. Gooley, H. Ebendorff-Heidepriem, High precision extrusion of glass tubes, Int. J. Appl. Glas. Sci. 10 (2019) 172–180. https://doi.org/10.1111/ijag.13092.